Electrostatic Atlas of Noncovalent Interactions Built in Metal-Organic Frameworks

Zhe Ji[1,4,6,*], Srijit Mukherjee[1,6], Jacopo Andreo[2], Anna Sinelshchikova[2], Francesca Peccati[3], Stefan Wuttke[2,5,*], and Steven G. Boxer[1,*]

[1] Department of Chemistry, Stanford University, Stanford, CA, USA.

[2] Basque Centre for Materials, Applications & Nanostructures (BCMaterials), Leioa, Spain.

[3] Center for Cooperative Research in Biosciences (CIC bioGUNE), Derio, Spain.

[4] Current address: College of Chemistry and Molecular Engineering, Peking University, Beijing, China.

[5] Current address: Academic Centre for Materials and Nanotechnology, AGH University of Krakow, Krakow, Poland.

[6] These authors contributed equally: Zhe Ji and Srijit Mukherjee.

[*] Correspondence to: jizhe@pku.edu.cn; swuttke@agh.edu.pl; sboxer@stanford.edu.

Abstract

Noncovalent interactions form the basis of matter and life yet are difficult to characterize. Here we devised a platform strategy to systematically build noncovalent interactions with selective chemical groups into precisely designed configurations by using metal-organic frameworks (MOF) as the molecular scaffold. Using the vibrational Stark effect benchmarked against computer models, we found the electric field provides a unifying metric for quantifying diverse noncovalent interactions in MOFs and solutions. By synthetically making and spectroscopically testing a collection of noncovalent interactions using a nitrile probe, we identified stabilizing fields as strong as -123 MV/cm produced additively by multiple hydrogen bonds, an unusual destabilizing field of +6 MV/cm between antiparallel dipoles , anomalous hydrogen-bond blueshifts as large as 34 cm^{-1}, and unique solvation under nanoconfinement. This method for making and testing noncovalent interactions opens new avenues for exploring the universe of noncovalent interactions.

Introduction

Noncovalent interactions are fundamental, ubiquitous forces that shape the properties and behaviors of molecules and their assemblies. These interactions can occur between any chemical groups that happen to get close enough, so there exists an enormous diversity of noncovalent interactions. While interactions such as hydrogen bonds are relatively strong and have well-defined and well-characterized properties, it is challenging to define most interactions which are non-specific and weak, even though their combination is often energetically significant. Two significant experimental challenges must be overcome to assess individual non-covalent interactions: first how to systemically build individual noncovalent interactions between specific groups at precisely defined geometries without any direct covalent connection, and second how to quantify these interactions from a physical perspective. We develop a general platform for placing selective chemical groups at defined positions and orientations using a metal-organic framework (MOF)[1-3], inspired by the molecular vise approach developed by Deng and co-workers[4-6]. We then use the vibrational Stark effect (VSE)[7-11] to measure the electric fields associated with these precisely designed interactions and characterize the electrostatic contribution to these interactions. We refer to the chemical group that produces the electric field of interest as the electric field donor and the group that experiences the field as the acceptor, a nomenclature inspired by the commonly used hydrogen-bond (H-bond) donor/acceptor and here applied to non-covalent interactions in general.

Previous studies have employed vibrational probes to report the electric fields associated with diverse chemical environments including proteins[10-23], lipid membranes[24,25], solvation shells[11,26,27], and electrode-electrolyte interfaces[28,29]. Although these results have provided insights into specific interactions, especially those related to a significant contribution of electrostatic preorganization to the proficiency of enzymes, the chemical scope is limited because in solution and at interfaces, the positioning of donor and acceptor typically cannot be controlled, and in biomolecules, the range of electric field donors is largely constrained by bio-specificity evolved from nature. We overcome these limitations by using a rigid scaffold onto which an electric field probe (nitrile) is anchored in apposition to a series of field donors (Fig. 1). Specifically, a MOF is employed to act as the structural backbone to hold the electric field donors and a nitrile acceptor as a probe in place. The permanent porosity of the MOF allows for the removal of solvent and isolation of the interrogated noncovalent interaction. Re-addition of solvent within this framework also provides a unique opportunity to examine solvation under nanoconfinement.

We chose a nitrile as the field probe because its vibrational frequencies lie in a part of the vibrational spectrum that is distinctly separate from background absorption, and nitriles have been extensively studied for probing electric fields[12-17]. Using a calibration based on vibrational solvatochromism, perturbations to the nitrile vibrational frequency within the MOF scaffold in response to different apposing functionalities can be used to extract the electrostatic contribution to the interactions. The experimental results are then compared with *ab initio* calculations, to interrogate and benchmark noncovalent interactions involving H-bonds and solvation effect under MOF-confinement.

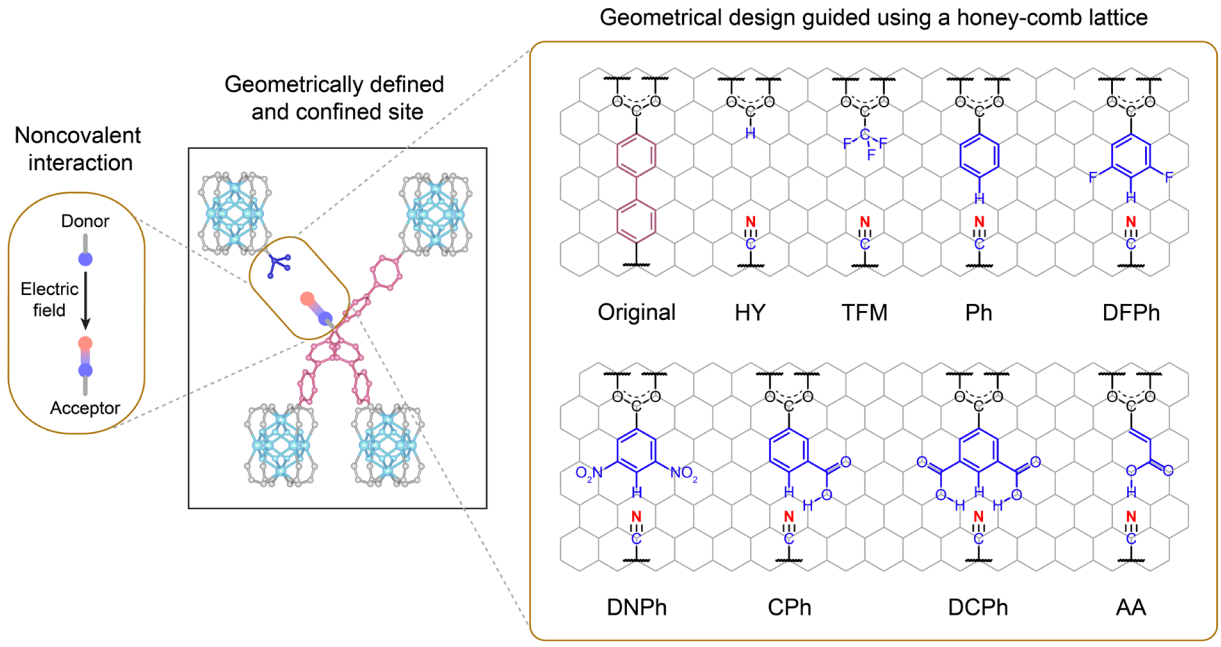

Fig. 1. Electrostatic picture of noncovalent interactions and the molecular platform developed in this work. To study the electric fields produced by noncovalent interactions, we anchored a nitrile probe (field acceptor) against a series of field donors in a geometrically defined and confined site in a metal-organic framework (MOF). The field donor can be systematically varied by geometrical design guided and visualized using a honey-comb lattice, resulting in an array of noncovalent interactions to be probed. HY denotes a structure containing a hydrogen atom as the field donor, TFM a trifluoromethyl donor, Ph a phenyl donor, DFPh a difluorophenyl donor, DNPh a dinitrophenyl donor, CPh a carboxylate phenyl donor, DCPh a dicarboxylate phenyl donor, and AA an acrylic acid donor.

Results and Discussion

Design and synthesis of MOFs holding field donor-acceptor pairs

We chose PCN-521[30] as the MOF scaffold for positioning field donor-acceptor pairs (Fig. 2), the same MOF that Deng and coworkers developed for the molecular vise approach[4-6], due to ease of functionalization and right size of the functionalization site. Single octahedral PCN-521 crystals (Fig. S1) were synthesized by first mixing and sonicating $ZrCl_4$ (metal source), 4,4,4,4-methanetetrayltetrabiphenyl-4-carboxylic acid (H_4L, organic linker), and trifluoroacetic acid (modulator) in diethylformamide (solvent) until a homogeneous suspension of the reactants was achieved. The mixture was then heated at 120°C for 22 hours and allowed to slowly cool to room temperature. During the reaction, $Zr_6O_4(OH)_4$ clusters (Fig. 2a, blue) were formed *in situ*, each providing 8 sites of coordination for extension[30]. Through the formation of Zr-carboxylate coordinate bonds, the cuboid Zr clusters are connected by the tetrahedral H_4L (Fig. 2a, green) into an extended network in a fluorite topology (Fig. 2b). The PCN-521 crystals were washed sequentially with dimethylformamide, methanol, acetone, hexane, and perfluoropentane before evacuation under high vacuum to empty the pore inside the PCN-521 structure. This process was optimized to prevent collapse of the MOF due to surface tension. The crystallinity and

the composition were confirmed by powder X-ray diffraction (PXRD) (Fig. S2) and digestion NMR spectroscopy (Fig. S3), respectively.

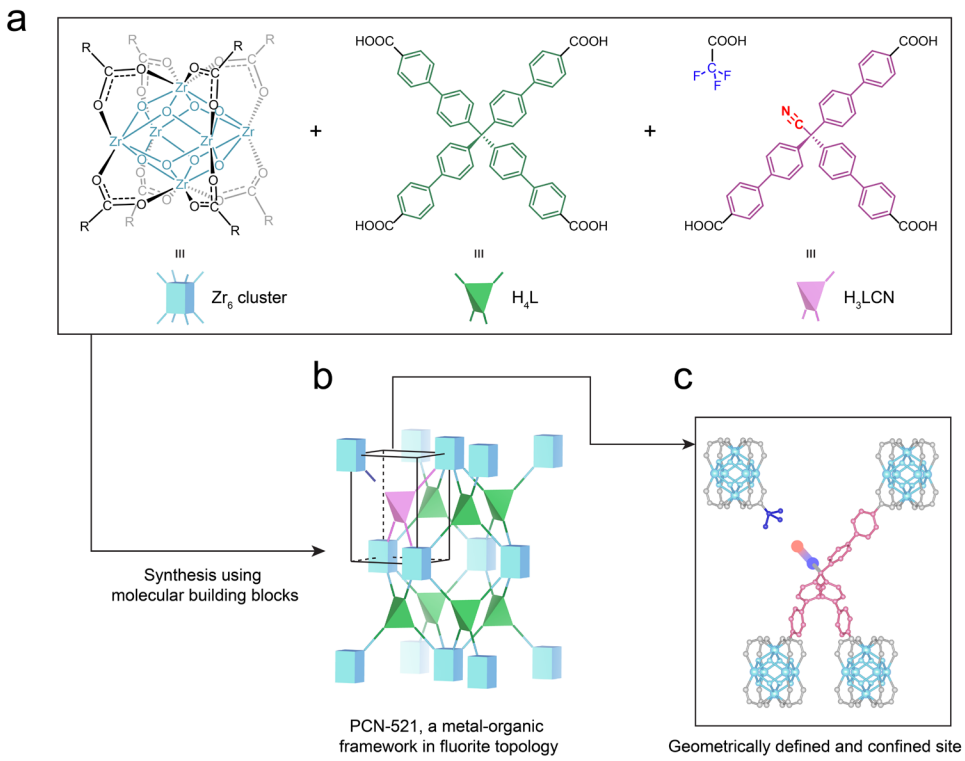

Fig. 2. PCN-521, a MOF, acts as a molecular scaffold onto which field donors and acceptors are installed in fixed configurations. (a) Molecular building blocks of the MOF. **(b)** Connection of the metal cuboid (Zr_6 cluster) and the organic tetrahedron (H_4L) into a network in fluorite topology. **(c)** Incorporation of the trigonal organic linker (H_3LCN) builds into the MOF crystals defective sites comprising a field donor ($-CF_3$) oriented towards a field acceptor (nitrile probe).

To install a vibrational probe into the structure of PCN-521, we designed and synthesized a trigonal pyramidal organic linker, tris-(4,4',4''-carboxylbiphenyl)-acetonitrile (H_3LCN, Fig. 2a, magenta) (Fig. S4-S11), which maintains three of the carboxylate ligands in H_4L and bears a nitrile probe in the fourth position, facing into the pore. The formation of PCN-521 has been proven robust enough to tolerate this partial replacement (up to 50% of H_4L with 3-connected ones)[4]. We found that a 2:1 molar ratio of H_4L to H_3LCN in the reaction mixture led to a 4:1 molar ratio of H_4L to H_3LCN in the obtained PCN-521 crystals, as measured by digestion NMR spectroscopy (Fig. S12, Table S1). The incorporation of H_3LCN does not compromise the overall crystallinity of PCN-521, as evidenced by the unchanged PXRD pattern (Fig. S13). The structural consequence of the linker substitution is that a fraction of the tetrahedral sites now has one biphenylene ligand replaced by a defined defect (Fig. 2b). On the opposite side, appended from the under-connected Zr cluster, is the trifluoracetic acid modulator added in the reaction mixture, so the PCN-521 structure has abundant defect sites that comprise the $-CF_3$ group aligned towards the nitrile (Fig. 2c). After washing and evacuation, the intentionally created defect sites are free of solvent, hosting a specific noncovalent interaction between $-CF_3$ and the nitrile in isolation.

The molecular and modular nature of the MOF structure allows us to systematically replace the trifluoroacetic acid with a range of other carboxylate ligands (Fig. 1). The MOF crystals were soaked in

methanol solutions of different carboxylic acid (~0.1 M) for 6 hours. The solution was changed two times during this period. The new carboxylic acid spontaneously substituted trifluoracetic acid, yielding a series of MOF variants we refer to as HY, TFM (as synthesized), Ph, DFPh, DNPh, CPh, DCPh, and AA, each bearing a unique field donor as shown in Fig. 1. The field donors were found to occupy 60-80% of the total open coordination sites as quantified by digestion NMR spectra (Fig. S14-S20, Table S1, Supplementary Text 5). Crystallinity of these MOF variants were confirmed by PXRD (Fig. S13).

Electrostatic characterization of aprotic interactions via the vibrational Stark effect

Previous work has established that nitrile vibrational probes exhibit a linear vibrational Stark effect, vibrational frequency shifts in proportion to the magnitude of electric field, in aprotic environments[8,26]. This does not extend to nitrile frequencies in protic (H-bonding) environments due to well-known anomalous blueshifts in frequency (Supplementary Text 4). Infrared (IR) absorption transition dipole moments (TDMs) of nitriles have been shown to exhibit linearity with the field in all environments[16]; however, this requires precise information on the absolute concentration of the nitrile, which is not applicable to the MOF powder samples studied here (Supplementary Text 4). In this work we focus on using the nitrile's vibrational frequency to infer the magnitude of electric fields.

To calibrate the sensitivity of the nitrile's frequency shifts to electric fields (the Stark tuning rate, $\Delta\vec{\mu}$), we employed triphenylacetonitrile (TPAN) as the model compound for measuring vibrational solvatochromism in aprotic solvents of varying polarity. TPAN's frequency shifts in response to solvent polarity were plotted against the solvent electric field magnitudes calculated by molecular dynamics simulations using AMBER (fixed-charge) and AMOEBA (polarizable) force-fields (Fig. S21-S24, Tables S2-S4). Compared with AMBER force fields, AMOEBA force fields, which incorporate molecular polarizability, consistently led to solvent electric fields with larger magnitudes, providing a $\Delta\vec{\mu}$ of 0.28 cm^{-1}/(MV/cm). This value is in close agreement with $\Delta\vec{\mu}$ of ~0.3 cm^{-1}/(MV/cm) obtained by DFT-based *in-silico* Stark calculations where a uniform field was applied along the direction of the nitrile in TPAN (Fig. S25). These results, together with recent study on nitrile-probed electric fields in photoactive yellow proteins[16,17,31], reinforce that polarizability is an indispensable parameter for accurate field calculations for nitrile probes. To confirm that TPAN is a valid model compound whose nitrile has similar Stark behavior as the nitrile probe installed in the MOF, for the *in-silico* Stark calculation we applied geometrical constraints to TPAN that the MOF backbone exerts on the incorporated H_3LCN (Fig. S25) and found that this only slightly perturbed $\Delta\vec{\mu}$ (Fig. S26). The consistent $\Delta\vec{\mu}$ between TPAN and H_3LCN observed from solvatochromism (Fig. S21, Table S5,S6) corroborates the validity of using TPAN as the model compound.

Raman spectroscopic measurements of the MOF crystals reveal vibrational frequencies of the nitrile in HY as 2243.2 cm^{-1}, with a 3.5 cm^{-1} blueshift compared to the nitrile model compound in hexanes (2239.7 cm^{-1}) (Fig. 3a, Fig. S27, Table S7). The installed field donor -H is measured to be 6.23 Å from the N atom in the nitrile based on DFT optimized structures (Fig. S28, Table S8,S9), positioning it beyond a range conducive for meaningful H-bond interactions with the nitrile. The absence of an H-bond indicates that the blueshift corresponds to an electric field smaller than that in hexane, essentially the gas phase frequency in the evacuated porous structure. To test the dependence of the blueshift on porosity, we applied harsh evacuation conditions to induce structural collapse and loss of crystallinity and observed that the nitrile peak broadens and red shifts by 3.4 cm^{-1} (Fig. S29). Next, we measured the vibrational frequency of the TFM variant, where the $-CF_3$ group aligns its dipole antiparallel to that of the nitrile; this resulted in a bluer nitrile vibration observed at 2245.1 cm^{-1} (Fig. 3b). The Ph variant — where the *para* H in the phenyl moiety is located significantly closer to the N atom in the nitrile (2.45 Å) — displayed a redshift to 2240.0 cm^{-1}.

With two -F groups added to the -Ph group, the DFPh variant displayed vibrational frequency of 2239.7 cm^{-1} (Fig. 3c), a small redshift manifesting a weak inductive effect of the -F substituents.

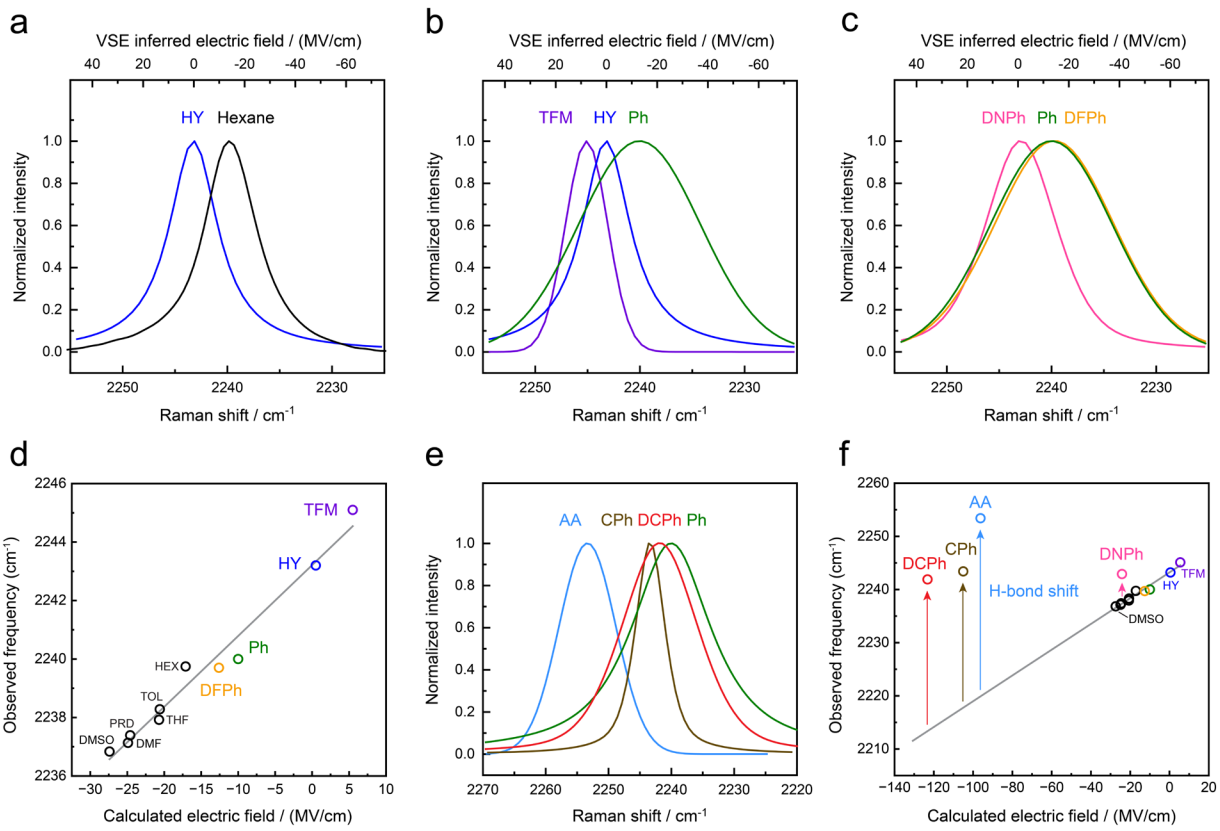

Fig. 3. Raman spectroscopy and electric field calculation for the MOF structures. (a) Fitted Raman spectrum for HY overlaid with the infrared spectrum of the TPAN model compound in hexane (raw spectra shown in Fig. S27; fitting results listed in Table S7). **(b)** Fitted Raman spectra for the HY, TFM, and Ph variants. **(c)** Fitted Raman spectra for the Ph, DFPh, and DNPh variants. **(d)** Field-frequency correlation plotted using electrostatic potential (ESP) calculated electric fields and experimentally measured Raman shifts for MOF variants and AMOEBA derived electric fields and experimentally measured infrared frequency for TPAN in various solvents, where HEX, TOL, THF, PRD, DMF, DMSO stand for hexanes, toluene, tetrahydrofuran, pyridine, *N,N'*-dimethylformamide, dimethyl sulfoxide, respectively. The linear fitting gives $\bar{\nu} = 0.242F + 2243.2$, with $r^2 = 0.97$, where $\bar{\nu}$ is the wavenumber (cm^{-1}) of the C≡N vibration, and F is the magnitude of electric fields (MV/cm) projected on the C≡N bond axis. The same equation is used to generate the top electric field axes in panel a-c. **(e)** Fitted Raman spectra for the Ph, CPh, DCPh, and AA variants. **(f)** Addition of observed Raman frequencies and calculated fields for CPh, DCPh, and AA onto the linear VSE plot from aprotic solvents and non-H-bond donors shown in **(d)** (note the expanded horizontal axis). The vertical deviations from the VSE line are attributed to the H-bond blueshifts.

To understand the observed vibrational shifts, we conducted *ab initio* geometry optimization of the MOF structures using the native PCN-521 crystal structure[30] (CCDC: DITJOH) as the starting model. We then incorporated H_3LCN and the field donors into the structure and find optimized geometries with no imaginary frequencies. From these geometries, we generated electrostatic potential (ESP) maps for the

interactions between the field donors and the nitrile to estimate the fields (details of the methodology to estimate fields are provided in the supplementary text S6 and Fig. S30). The field calculations from ESP show that the -H in HY produces a negligible field of 0.5 MV/cm on the nitrile, while the -Ph and -3,5-difluoroPh produces a stabilizing field of -10 MV/cm and -12.6 MV/cm, respectively (Table S10). The electric field exerted by the $-CF_3$ group is confirmed to be destabilizing and calculated to be +5.5 MV/cm. In Fig. 3d, we plot the electric field magnitudes of these interactions against the nitrile vibrational frequencies from the Raman measurements.

Overlay of the MOF datapoints with TPAN solvatochromism datapoints (AMEOBA) reveals a unifying linear correlation with a $\Delta\vec{\mu}$ of 0.242 cm^{-1}/(MV/cm) and an intercept at 2243.2 cm^{-1}. The good linearity ($r^2 = 0.97$) indicates that the averaged electric fields produced by solvents and the oriented electric fields exerted by chemical groups installed in the MOF have the same physical foundation, manifesting the power of electric field, a unifying metric for quantifying diverse noncovalent interactions in MOFs and solutions (and proteins) with a common unit. Using the MOF as a platform, we built very low-field chemical environments approaching that in gas phase, a system unattainable by solvation or protein environments. The unifying linear correlation shown in Fig.3d also showcases that AMOEBA forcefields that employ an extensive electrostatic description for solvents and ESP maps based on a quantum mechanical approach for the MOFs, two different computational methods, now converge into a precise prediction of electric fields. Using the new calibration curve, we add a top axis to Fig. 3a-c to map the readout of the nitrile vibrational frequency to the magnitude of electric fields inside the MOF.

Anomalous blueshift in frequency due to H-bond formed by protic field donors

With the robust VSE established, we set out to build and interrogate systems involving H-bonds to the nitrile. We installed field donors bearing protic moieties, CPh, DCPh, and AA, displaying vibrational frequencies of 2243.4 cm^{-1}, 2241.9 cm^{-1}, and 2253.4 cm^{-1}, respectively (Fig. 3e). DFT-based geometry optimization of these structures reveals conformational heterogeneity due to bond rotations within these donors; however, all with a dominant ground state conformer (based on Boltzmann populations at 298K) directly H-bonded to the nitrile in rather short heavy atom distances (< 3 Å) and near head-on angles (> 150º) (Fig. S28, Table S8, S9). The Boltzmann-averaged ESP fields for CPh, DCPh, AA are calculated as -105.0, -123.2, and -96.2 MV/cm (Table S11) — fields of magnitudes that are typically encountered in enzyme active sites and important for catalysis. In Fig. 3f we add the observed Raman frequencies and calculated fields for CPh, DCPh, and AA onto the linear VSE plot from aprotic solvents and non-H-bond donors (Fig. 3d). We attribute the striking deviation from the VSE line to the H-bond blueshifts ($\Delta\bar{\upsilon}_{HB}$), which are 25.6, 28.6, and 33.5 cm^{-1} for CPh, DCPh and AA, respectively (Table S11). These values of $\Delta\bar{\upsilon}_{HB}$ in the MOF match those predicted with a model used to explain the vibrational frequencies of nitriles embedded in photoactive yellow protein (PYP), where $\Delta\bar{\upsilon}_{HB}$ can be predicted depending on the heavy atom distances, e.g. N-O distance in C≡N---H—O, and the heavy atom angles, e.g. C-N-O angle in C≡N---H—O (unpublished[31]). Interestingly, because here we build H-bonds in the MOFs that are shorter and more head-on than those observed in the high resolution structures of nitrile-substituted PYPs, we observed $\Delta\bar{\upsilon}_{HB}$ larger than any of those in the PYP variants. Note that both IR frequency and intensity tuning were used for the analysis of fields in PYP variants because the concentration is known accurately, but this is not the case with sufficient precision for the MOF systems. Furthermore, the intensities of Raman spectra depend on multiple factors, and only an approximate concentration of the nitrile in the MOF can be estimated using digestion NMR. Despite this, the MOF system acts as an excellent experimental platform for building and probing short and head-on hydrogen bonds.

We further sought to test whether a weak H-bond can be built into the MOF by using -3,5-dinitrophenyl moiety as the field donor. It has a slightly acidic C-H group due to the strong electron-withdrawing nitro substituents, and the DNPh variant exhibits a vibrational frequency of 2242.0 MV/cm (Fig. 3c). We calculated the ESP field for DNPh as -24.2 MV/cm, resulting in a $\Delta\bar{\nu}_{\mathrm{HB}}$ of 5.6 cm^{-1} (Table S11), lying at the smallest end of the $\Delta\bar{\nu}_{\mathrm{HB}}$ spectrum, consistent with chemical intuition.

Unique solvation under nanoconfinement

We extended the use of the MOF platform to examine unique solvation environments confined in the MOF pore. The nitrile probe is located at the shared window between 3 octahedral cavities, each of which, with a size of 20.5×20.5×37.4 Å[30], can potentially be filled with about 100 DMSO molecules. After evacuation, we soaked nitrile-containing MOF crystals in DMSO and measured their Raman spectra. DMSO was selected due to its low vapor pressure and high boiling point, which reduced solvent evaporation in the experimental scheme of our Raman measurements. Upon DMSO solvation, the nitrile in HY showed a redshift by 2.9 cm^{-1} with respect to the solvent-free HY (Fig. 4a), corresponding to a more stabilizing electric field by –12.0 MV/cm (Table S12). Given that the TPAN's nitrile in bulk DMSO experiences an averaged field of -27.4 MV/cm, the DMSO filled in the MOF pore constitutes a unique solvation environment that produces less than half of the electric field that bulk DMSO does. The solvation environment was also found to be field-donor dependent. The TFM variant displays a redshift by 5.7 cm^{-1} after DMSO solvation, corresponding to an electric field change by -23.5 MV/cm (Fig. 4b), while the Ph variant exhibits a redshifts by only -1.3 cm^{-1}, corresponding to an electric field change by -5.4 cm^{-1} (Fig. 4c). This minimal stabilization can be explained by the bulky -Ph group near the nitrile, leaving little space for the solvent to form an effective solvation sphere.

To investigate how solvation perturbs H-bond, we soaked the AA variant in DMSO and observed a dramatic redshift of the nitrile frequency by 14.3 cm^{-1} (Fig. 4d), indicating disappearance of the large H-bond blueshift (33.5 cm^{-1}) characteristic of AA. Assuming no hydrogen bond remains, the vibration shift of DMSO-soaked AA can be treated using the purely electrostatic model, resulting in a more destabilizing electric field by 79.2 MV/cm, a big loss of the stabilizing field due to the removal of the strong H-bond. The electrostatic effect of solvation in the MOF variants are summarized in Fig. 4e, providing a quantitative description of solvation under MOF-nanoconfinement.

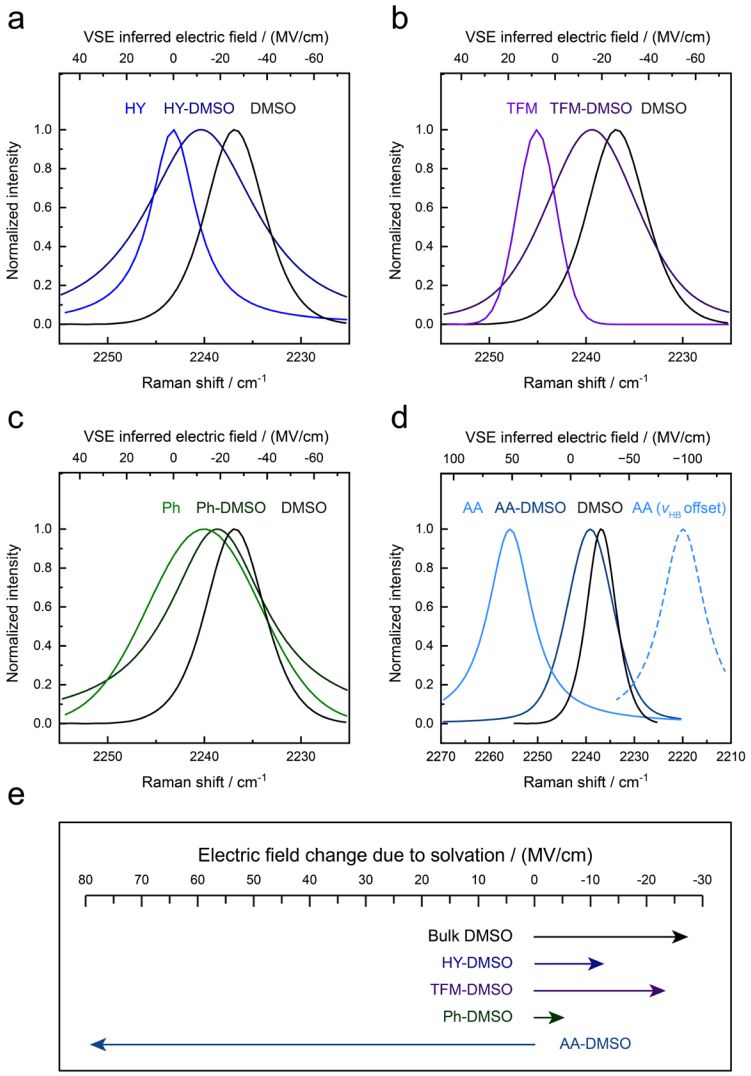

Fig. 4. Spectroscopic observation and electrostatic quantification of solvation under nanoconfinement. **(a)** Fitted Raman spectra for evacuated HY and the DMSO solvated HY, overlaid with the infrared spectrum of TPAN in DMSO. **(b)** Fitted Raman spectra for the TFM variant and the DMSO solvated TFM variant, overlaid with the infrared spectrum of TPAN in DMSO. **(c)** Fitted Raman spectra for the Ph variant and the DMSO solvated Ph variant, overlaid with the infrared spectrum of TPAN in DMSO. **(d)** Fitted Raman spectra for the AA variant and the DMSO solvated AA variant, overlaid with the infrared spectrum of TPAN in DMSO. The dotted line plots an hypothetical AA spectrum as if there is no H-bond blueshift. **(e)** Changes in the nitrile experienced electric field due to DMSO solvation.

Conclusion

In summary we have shown that the PCN-521 MOF framework can be used as a general platform to create a series of noncovalent interactions using a modular molecular approach. The synthesized noncovalent interactions were interrogated by Raman spectroscopy and interpreted within the framework of the vibrational Stark effect giving the electric fields a donor exerts onto an acceptor. We found that the electric fields associated with noncovalent interactions are highly diverse, from being as destabilizing as +6 MV/cm

to being as stabilizing as -123 MV/cm. The electric field provides an absolute, quantitative metric enabling broad comparisons across various chemical groups in terms of their electrostatic properties. Using the platform, we identified electric fields as weak as those in gas phase and H-bonds that are stronger than those in certain proteins. We further studied the noncovalent interactions involved in solvation by utilizing the microporous structure of the MOF to create solvent organizations that are inaccessible by the bulk. These results and analysis not only address fundamental questions about elementary interactions in chemistry, biology, and material sciences, but also provide useful tools for molecular design and engineering.

Acknowledgements

This work was supported by the International Human Frontier Science Program Organization (RGP0047/2022) and, in part, by NIH grant GM118044 (to SGB). Part of this work was performed at the Stanford Nano Shared Facilities (SNSF), supported by the National Science Foundation under award ECCS-2026822.We would also acknowledge the use of services from the Stanford Sherlock HPC facility. We thank Gonzalo Jimenez-Oses for discussions related to the cluster-based DFT calculations of the PCN-521 scaffold. We thank Jacob Kirsh, Jacek Kozuch, Steven Fried and Mojgan Asadi for discussions.

Author contributions

Z.J., S.W., and S.G.B. designed the research. Z.J. and S.M. performed most of the experiments and data analysis, including MOF synthesis, PXRD measurements, NMR spectroscopy, Raman spectroscopy, infrared spectroscopy. S.M. and F.P. performed computation. A.S. and J.A. synthesized the H_3LCN linker and supported the MOF synthesis. Z.J., S.M., J.A., S.W., and S.G.B discussed the results. Z.J., S.M., S.W., and S.G.B wrote the manuscript.

Corresponding authors

Correspondence to Zhe Ji (jizhe@pku.edu.cn), Stefan Wuttke (swuttke@agh.edu.pl), Steven G. Boxer (sboxer@stanford.edu).

Competing interests

The authors declare no competing interests.

References

1 Furukawa, H., Cordova, K. E., O'Keeffe, M. & Yaghi, O. M. The Chemistry and Applications of Metal-Organic Frameworks. *Science* **341**, 1230444 (2013). https://doi.org/10.1126/science.1230444

2 Li, H., Eddaoudi, M., O'Keeffe, M. & Yaghi, O. M. Design and synthesis of an exceptionally stable and highly porous metal-organic framework. *Nature* **402**, 276-279 (1999). https://doi.org/Doi 10.1038/46248

3 Freund, R. *et al.* 25 Years of Reticular Chemistry. *Angew Chem Int Edit* **60**, 23946-23974 (2021). https://doi.org/10.1002/anie.202101644
4 Wang, Y., Liu, Q., Zhang, Q., Peng, B. & Deng, H. X. Molecular Vise Approach to Create Metal-Binding Sites in MOFs and Detection of Biomarkers. *Angew Chem Int Edit* **57**, 7120-7125 (2018). https://doi.org/10.1002/anie.201803201
5 Yan, W. *et al.* Molecular Vises for Precisely Positioning Ligands near Catalytic Metal Centers in Metal-Organic Frameworks. *J Am Chem Soc* **142**, 16182-16187 (2020). https://doi.org/10.1021/jacs.0c07450
6 Chen, W. H. *et al.* Precise Distance Control and Functionality Adjustment of Frustrated Lewis Pairs in Metal-Organic Frameworks. *J Am Chem Soc* **146**, 12215-12224 (2024). https://doi.org/10.1021/jacs.4c03133
7 Chattopadhyay, A. & Boxer, S. G. Vibrational Stark-Effect Spectroscopy. *J Am Chem Soc* **117**, 1449-1450 (1995). https://doi.org/DOI 10.1021/ja00109a038
8 Fried, S. D. & Boxer, S. G. Measuring Electric Fields and Noncovalent Interactions Using the Vibrational Stark Effect. *Accounts Chem Res* **48**, 998-1006 (2015). https://doi.org/10.1021/ar500464j
9 Park, E. S., Andrews, S. S., Hu, R. B. & Boxer, S. G. Vibrational stark spectroscopy in proteins: A probe and calibration for electrostatic fields. *J Phys Chem B* **103**, 9813-9817 (1999). https://doi.org/DOI 10.1021/jp992329g
10 Fried, S. D., Bagchi, S. & Boxer, S. G. Extreme electric fields power catalysis in the active site of ketosteroid isomerase. *Science* **346**, 1510-1514 (2014). https://doi.org/10.1126/science.1259802
11 Fried, S. D., Bagchi, S. & Boxer, S. G. Measuring Electrostatic Fields in Both Hydrogen-Bonding and Non-Hydrogen-Bonding Environments Using Carbonyl Vibrational Probes. *J Am Chem Soc* **135**, 11181-11192 (2013). https://doi.org/10.1021/ja403917z
12 Suydam, I. T., Snow, C. D., Pande, V. S. & Boxer, S. G. Electric fields at the active site of an enzyme: Direct comparison of experiment with theory. *Science* **313**, 200-204 (2006). https://doi.org/10.1126/science.1127159
13 Slocum, J. D. & Webb, L. J. Measuring Electric Fields in Biological Matter Using the Vibrational Stark Effect of Nitrile Probes. *Annu Rev Phys Chem* **69**, 253-271 (2018). https://doi.org/10.1146/annurev-physchem-052516-045011
14 Fafarman, A. T. & Boxer, S. G. Nitrile Bonds as Infrared Probes of Electrostatics in Ribonuclease S. *J Phys Chem B* **114**, 13536-13544 (2010). https://doi.org/10.1021/jp106406p
15 Yang, Y. Y., Feng, R. R. & Gai, F. 4-Cyanotryptophan as a Sensitive Fluorescence Probe of Local Electric Field of Proteins. *J Phys Chem B* **127**, 514-519 (2023). https://doi.org/10.1021/acs.jpcb.2c07605
16 Weaver, J. B., Kozuch, J., Kirsh, J. M. & Boxer, S. G. Nitrile Infrared Intensities Characterize Electric Fields and Hydrogen Bonding in Protic, Aprotic, and Protein Environments. *J Am Chem Soc* **144**, 7562-7567 (2022). https://doi.org/10.1021/jacs.2c00675
17 JM, K., JB, W., SG, B. & J, K. Comprehensive analysis of nitrile probe IR shifts and intensities in proteins: experiment and critical evaluation of simulations. *ChemRxiv*, doi:10.26434/chemrxiv-22023-j26935v-v26432 (2024).
18 Yang, Y. Y., Liu, J. S., Feng, R. R., Zhang, W. K. & Gai, F. C N Stretching Frequency as a Convenient Reporter of Charge Separation in Molecular Systems. *J Phys Chem B* **127**, 6999-7003 (2023). https://doi.org/10.1021/acs.jpcb.3c02707
19 Du, J. J., Wang, H. M. & Wei, L. Bringing Vibrational Imaging to Chemical Biology with Molecular Probes. *Acs Chem Biol* **17**, 1621-1637 (2022). https://doi.org/10.1021/acschembio.2c00200

20 Schneider, S. H., Kozuch, J. & Boxer, S. G. The Interplay of Electrostatics and Chemical Positioning in the Evolution of Antibiotic Resistance in TEM β-Lactamases. *Acs Central Sci* **7**, 1996-2008 (2021). https://doi.org/10.1021/acscentsci.1c00880

21 Ji, Z. *et al.* Protein Electric Fields Enable Faster and Longer-Lasting Covalent Inhibition of β-Lactamases. *J Am Chem Soc* (2022). https://doi.org/10.1021/jacs.2c09876

22 Ji, Z. & Boxer, S. G. β-Lactamases Evolve against Antibiotics by Acquiring Large Active- Site Electric Fields. *J Am Chem Soc* **144**, 22289-22294 (2022). https://doi.org/10.1021/jacs.2c10791

23 Zheng, C., Ji, Z., Mathews, I. I. & Boxer, S. G. Enhanced active-site electric field accelerates enzyme catalysis. *Nat Chem* (2023). https://doi.org/10.1038/s41557-023-01287-x

24 Shrestha, R., Cardenas, A. E., Elber, R. & Webb, L. J. Measurement of the Membrane Dipole Electric Field in DMPC Vesicles Using Vibrational Shifts of p-Cyanophenylalanine and Molecular Dynamics Simulations. *J Phys Chem B* **119**, 2869-2876 (2015). https://doi.org/10.1021/jp511677j

25 Hu, W. H. & Webb, L. J. Direct Measurement of the Membrane Dipole Field in Bicelles Using Vibrational Stark Effect Spectroscopy. *J Phys Chem Lett* **2**, 1925-1930 (2011). https://doi.org/10.1021/jz200729a

26 Bagchi, S., Fried, S. D. & Boxer, S. G. A Solvatochromic Model Calibrates Nitriles' Vibrational Frequencies to Electrostatic Fields. *J Am Chem Soc* **134**, 10373-10376 (2012). https://doi.org/10.1021/ja303895k

27 Zheng, C. *et al.* A two-directional vibrational probe reveals different electric field orientations in solution and an enzyme active site. *Nat Chem* **14**, 891-+ (2022). https://doi.org/10.1038/s41557-022-00937-w

28 Sarkar, S., Maitra, A., Banerjee, S., Thoi, V. S. & Dawlaty, J. M. Electric Fields at Metal-Surfactant Interfaces: A Combined Vibrational Spectroscopy and Capacitance Study. *J Phys Chem B* **124**, 1311-1321 (2020). https://doi.org/10.1021/acs.jpcb.0c00560

29 Delley, M. F., Nichols, E. M. & Mayer, J. M. Electrolyte Cation Effects on Interfacial Acidity and Electric Fields. *J Phys Chem C* **126**, 8477-8488 (2022). https://doi.org/10.1021/acs.jpcc.2c01134

30 Zhang, M. W. *et al.* Symmetry-Guided Synthesis of Highly Porous Metal-Organic Frameworks with Fluorite Topology. *Angew Chem Int Edit* **53**, 815-818 (2014). https://doi.org/10.1002/anie.201307340

31 Kirsh, J. M. & Kozuch, J. Hydrogen bond blueshifts in nitrile vibrational spectra are dictated by hydrogen bonding geometry and dynamics. *To be published* (2024).